COMPARATIVE ANALYSIS OF MELT POOL EVOLUTION IN SELECTIVE LASER MELTING OF INCONEL 625 AND INCONEL 718 NICKEL-BASED SUPERALLOYS

M. Ben Slama[1], S. Chatti[1*], L. Kolsi[2,3]

[1]Laboratory of Mechanical Engineering (LGM), National Engineering School of Monastir (ENIM), University of Monastir, Rue Ibn El Jazzar, 5000 Monastir, Tunisia
[2]Department of Mechanical Engineering, College of Engineering, University of Ha'il, Ha'il City 81451, Saudi Arabia
[3]Laboratory of Metrology and Energy Systems, Department of Energy Engineering, University of Monastir, 5000 Monastir, Tunisia
*Corresponding author's e-mail address: sami.chatti@udo.edu

ABSTRACT

One of the key advantages of Additive Manufacturing is the versatility in working with a wide range of materials. Among these materials, Nickel-based superalloys have drawn great attention of specialists. This study investigates the behavior of Inconel 625 and Inconel 718 during selective laser melting. While these alloys have many similarities, thus their distinct chemical compositions determine different responses to this new process, which the authors aimed to elucidate in this study. Numerical simulations using ANSYS Additive® software were conducted to compare the melt pool dimensions (depth and width) of Inconel 625 and Inconel 718. The results reveal that the material's thermal properties play a significant role in determining the melt pool geometry. The Inconel 718 consistently exhibited larger melt pool dimensions than Inconel 625. The findings highlight the importance of understanding the connection between the material properties and process parameters.

KEYWORDS: Additive Manufacturing, selective laser melting, melt pool, Nickel-based superalloys, numerical simulation

1. INTRODUCTION

Additive Manufacturing (AM) is a revolutionary technology that creates a 3D product from a CAD file with no specific tooling. This layer-by-layer process allows the manufacturing of highly complex designs that could not be produced by conventional manufacturing methods [1]. Its advantages have widened the application of this technology in diversified fields, such as automotive, aerospace, tooling, medical and dental, etc. Hence, AM is not restricted to a unique material, but it covers a wide range of metallic and non-metallic materials [2].

Across the last two decades, there have been notable investigations on steels [3], Ti- [4], Mg- and Nickel [5]-based alloys [6]. Among this large selection of materials that could be processed by AM, specifically Selective Laser Melting (SLM), Nickel-based superalloys are the most extensively investigated superalloys in the field of AM [7].

Nickel-based superalloys have gained widespread popularity in various industries due to their exceptional properties, including excellent refractoriness and remarkable resistance to corrosion at both low and high temperatures [8]. For instance, Inconel 625 (IN625) has interesting properties, ideal fatigue, and creep strengths in addition to a high resistance to corrosion and oxidation. This alloy disposes remarkable weldability that encourages its application in several fields like aerospace, petrochemical, and marine industries.

As for the Inconel 718 (IN718) alloy, it is known for its high strength, creep resistance, and good fatigue life at elevated temperatures (higher than 700 °C). Thanks to its good weldability, high wear, and hot corrosion resistance, this alloy is used in several applications, such as aircraft engines, gas turbines, nuclear reactors, and turbocharger rotors [9]. However, manufacturing these alloys are challenging through conventional machining methods [10]. This is mainly attributed to the refractory element segregation at high temperatures [11]. This fact raised the need for advanced manufacturing techniques, mainly AM, for such superalloys [12].

Although these two alloys share common aspects and characteristics, they do have some differences in their chemical composition as presented in Table 1. Hence, they could display contrasting responses to the SLM process, which is yet explicitly uncovered.

Table 1. Chemical composition of Inconel 625 and Inconel 718

Alloys/ Elements	Cr [%]	Mo [%]	Nb [%]	Fe [%]	Al [%]	Ti [%]	C [%]	Mn [%]	Ni [%]	Co [%]
Inconel 625	20-23	8-10	3.15-4.15	≤5	≤0.4	≤0.4	≤0.1	≤0.5	Bal.	1
Inconel 718	17-21	2.8-3	4.8-5.5	Balance	0.2-0.8	0.65-1.15	≤0.1	0.35	50-55	1

This paper presents an investigation on the evolution of both IN625 and IN718 during selective laser melting. This comparison covers the relationship between the distinct responses of the two alloys and their characteristics and points to an easier selection of the appropriate material.

2. METHODS

The two Inconel alloys are compared using the dimensions (depth and width) of the melt pool created during SLM. These dimensions are obtained from numerical simulations performed on ANSYS additive ® software.

2.1. Model Description

The numerical model simulates the SLM of a single track with a length of 3 mm (Fig. 1). The heat equation (Equation 1) is solved through Ansys thermal solver using the Finite Element Method (FEM).

$$\rho C \left(\frac{\partial T}{\partial t} + \{v\}^T \{L\} \, T \right) + \{L\}^T \{q\} = \ddot{q} \qquad (1)$$

where ρ is the material density

C - specific heat
T - temperature
$\{q\}$ - heat flux vector
$\ddot{q}$ - heat generation rate per unit volume
$\{L\}$ - operator vector,
$\{v\}$ - the velocity vector for the mass transport of heat.

The laser beam has a Gaussian distribution and a diameter of 100 µm. The powder layer is modeled as a continuous medium with an assumed factor of 0.6 for the material properties. These latter properties are temperature-dependent. The mechanical and thermal material properties, for both Inconel alloys, are presented in Table 2, and the boundary conditions are summarized in Table 3.

2.2. Model Validation

To validate the numerical model, a series of numerical simulations, using combinations of laser power and scan speed, detailed in Table 4, was conducted. For this purpose, the experimental conditions reported by Andreotta in. [13] were used for this simulation. The experimental work, using IN718, was made at an ambient temperature (25 °C) and using a layer thickness of 40 µm.
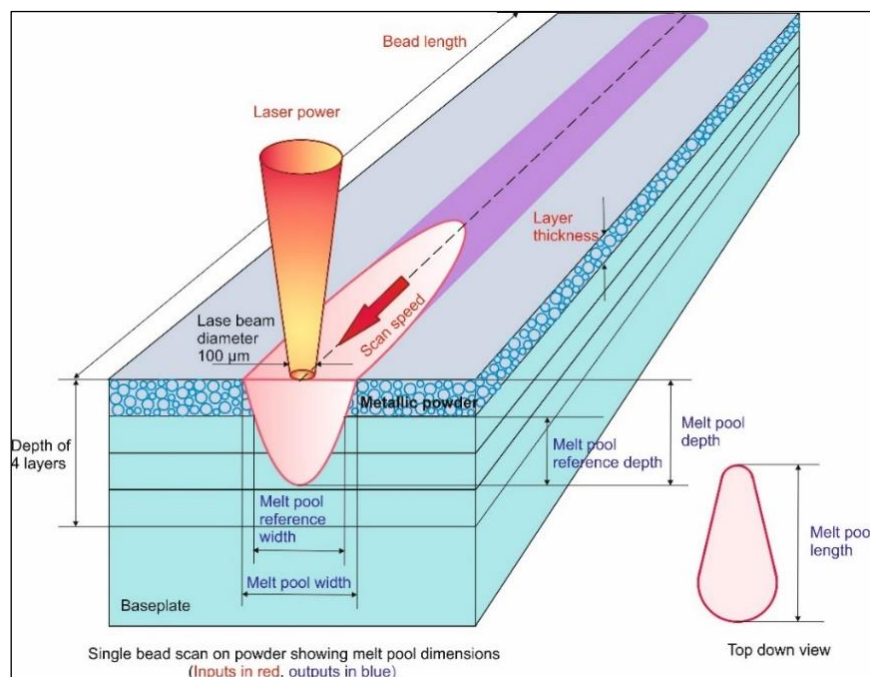
Fig 1. Schematic illustration of the numerical model

Table 2. Fixed material properties of Inconel 625 and Inconel 718

Alloys	Property	Inconel 625	Inconel 718
Mechanical properties	Elastic Modulus [GPa]	208	211
	Poisson ratio	0.33	0.3
	Material Yield strength [MPa]	480	1040
	Hardening factor	0.0041	0.0048
Thermal properties	Solid thermal conductivity at room temperature [W/ m °K]	9.8	11.4
	Solid density at room temperature [kg/m^3]	8440	8200
	Solid specific heat at room temperature [J/ kg K]	429	435
	Solidus temperature [°C]	1290	1260
	Liquidus temperature [°C]	1350	1340
	Thermal expansion coefficient [K^{-1}]	0.00001358	0.0000128

Table 3. Boundary conditions

Location	Boundary condition
Base plate	Fixed temperature
Top face	Uniform convection
Lateral faces	Adiabatic

Results in Table 4 reveal a good accuracy between experimental and numerical results, specifically at low scan speed. A deviation between the real and predicted values is expected and is mainly attributed to both numerical assumptions and experimental measurements.

As the scan speed rises, the difference between the calculated melt pool size and the reported melt pool size by Andretto et al. [13] rises. This could be attributed to the complicated physical phenomena (related to the fluid dynamics) that are not considered in our thermal model.

Table 4. Numerical and experimental results

Laser power [W]	Scan speed [mm/s]	Width [µm]		
		Experimental	Numerical	Error
150	700	118 ± 5.1	113	0.04
	1200	97 ± 8.1	64	0.34
200	700	144.5 ± 9.2	136	0.06
	1200	113.6 ± 11.9	92	0.19
300	700	185 ± 1.21	166	0.10
	1200	132 ± 10.6	124	0.06
	2200	104 ± 9	73	0.30
	2500	94 ± 16.9	58	0.38
Laser power [W]	Scan speed [mm/s]	Depth [µm]		
		Experimental	Numerical	Error
150	700	48.2 ± 11.3	45	0.07
	1200	34 ± 14.2	13	0.62
200	700	64.4 ± 18.2	71	0.10
	1200	41.5 ± 9.8	29	0.30
300	700	96.5 ± 24.7	119	0.23
	1200	101.1 ± 37.2	92	0.09
	2200	42 ± 8.8	18	0.57
	2500	39.9 ± 14.8	12	0.70

3. RESULTS AND DISCUSSION

After validating the model, the melt pool size (depth and width) of both IN718 and IN625 were predicted using different combinations of parameters from Table 5. Here, the base plate temperature is fixed at 80 °C to minimize the resulting residual stresses that could be generated during SLM.

Table 5. Process parameters used in the simulation

Parameter	Value
Layer thickness [μm]	50
Base plate temperature [°C]	80
Laser power [W]	50-100-150-200
Scan speed [mm/s]	500-1000-1500-2000

The melt pool depth and width evolutions for both Inconel alloys IN718 and IN625 are presented in figures 2, respectively 3. The continuous line refers to the IN718 and the discontinuous one refers to the IN625. In Figure 2, the continuous and discontinuous lines belonging to the lowest power (50 W) are superposed and have a horizontal evolution at a constant value of zero. This is attributed to the small melt pool created at this power that did not reach the substrate, in this case, the predicted depth equals zero. For the higher powers, the melt pool depth decreases as the scan speed increases, and at a fixed scan speed the depth increases as the power increases for both Inconel alloys.

These observations can also be noticed in the melt pool width evolution presented in figure 3. In fact, at a higher power more energy is absorbed by the material which generates a deeper and wider melt pool. On the other hand, at a fixed laser power, when the scan is accelerated, the interaction time is reduced. This means that at high scan speed, there is not enough time for the powder bed to absorb enough energy, therefore a small melt pool is created. These findings correlate well with the results reported by Khorasani et al. [14] and Kumar et al. [15].

The comparison between the evolution of the two Inconel alloys reveals that the melt pool depth of the IN718 is more important for all values of laser power and it decreases with an almost constant deviation. As for the melt pool width (figure 3), the same behavior is observed. This is mainly attributed to the difference in thermal properties of both alloys (summarized in Table 2). In fact, thermal properties play a crucial role in how materials melt and in the shape of their melt pool. It influences how heat propagates within a material and how the material reacts to heat. The primary thermal properties to consider is the thermal conductivity. The alloy with higher thermal conductivity, the IN718, transmits heat more efficiently than the IN625 with lower conductivity. Indeed, heat will propagate more rapidly within the material, potentially resulting in a more uniform melting.

It can also be depicted from figures 2 and 3 that the deviation in both width and depth between the IN718 and the IN625 is more important at higher powers. This observation is more meaningful and clearer in figure 4. The difference in dimensions between the two alloys is more important as the laser power increases. It increases from 6 to 12 μm, and from 4 to 16 μm for the melt pool depth, and respectively width. This is attributed to the input energy which is conspired as a determinant factor when comparing two materials. In fact, the amount of heat energy applied to the material determines how much it will melt and the depth of the melted pool. More heat input will result in a deeper melted pool.
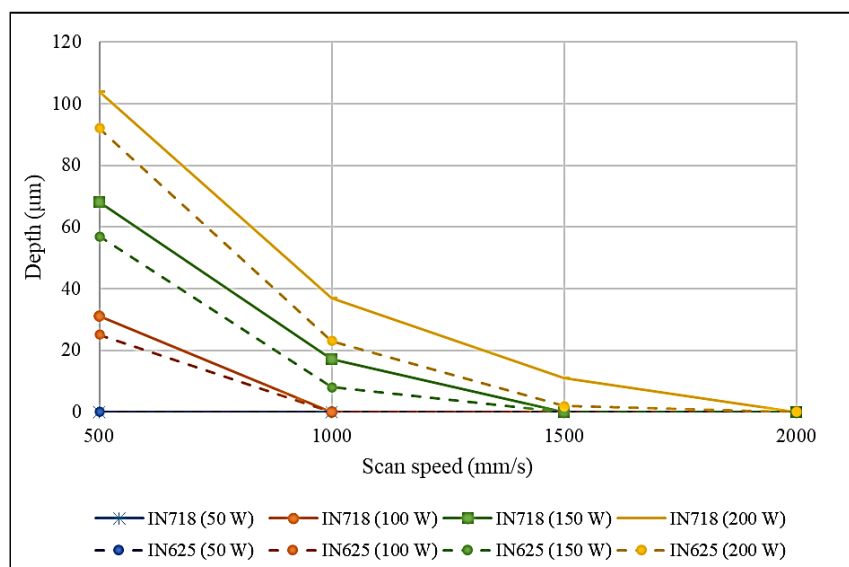
Fig 2. Melt pool depth evolution for Inconel 625 and Inconel 18 alloys
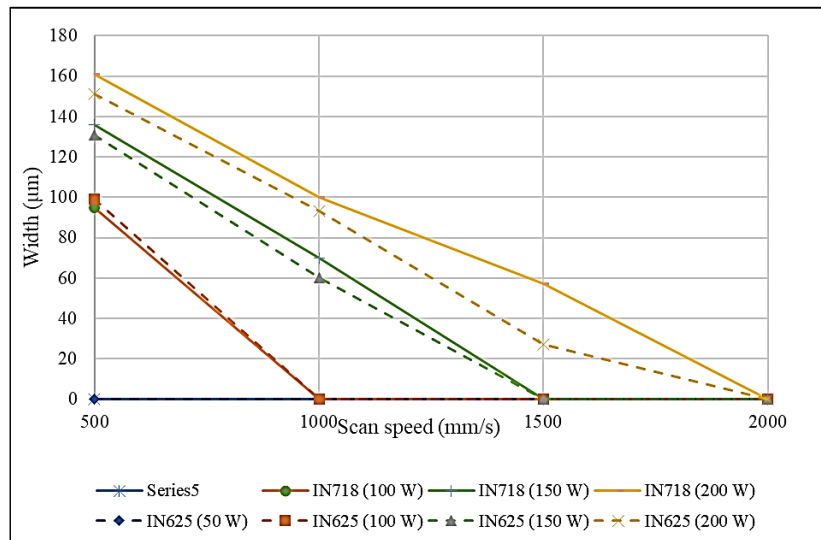
Fig 3. Melt pool width evolution for Inconel 625 and Inconel 718
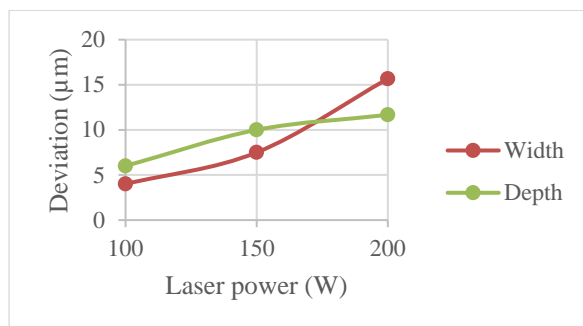
Fig 4. Deviations in the melt pool dimensions of the Inconel 625 and Inconel 718

4. CONCLUSIONS

This study was focused on the behavior of two prominent Nickel-based superalloys, IN625 and IN718, during the Selective Laser Melting (SLM) process. These alloys, known for their exceptional properties, find applications across various industries and their compatibility with AM technologies like SLM is of great interest.

The investigation focused on the melt pool dimensions (depth and width) of both alloys under different laser power and scan speed combinations. The results revealed notable differences in the melt pool characteristics between IN625 and IN718. IN718 consistently exhibited larger melt pools compared to IN625, irrespective of the parameter variations. The observed differences in melt pool dimensions can be attributed to the distinct thermal properties of the two alloys, particularly their thermal conductivity. IN718, with higher thermal conductivity, exhibited more efficient heat transfer, resulting in deeper and wider melt pools. Furthermore, the deviation between the two alloys' melt pool dimensions increased with higher laser powers, emphasizing the significance of input energy in the SLM process.

This study contributes valuable insights into the behavior of IN625 and IN718 during SLM, aiding in material selection for specific applications in additive manufacturing. It highlights the importance of considering material properties, laser parameters, and their impact on melt pool characteristics when employing AM techniques with Nickel-based superalloys.

REFERENCES

[1] **Maamoun A. H., Xue Y. F., Elbestawi M. A., Veldhuis S. C.,** *Effect of selective laser melting process parameters on the quality of al alloy parts: Powder characterization, density, surface roughness, and dimensional accuracy*, Materials, Vol. 11(12), 2018, doi: 10.3390/ma11122343.

[2] **Ngo T. D., Kashani A., Imbalzano G., Nguyen K. T. Q., Hui D.,** *Additive manufacturing (3D printing): A review of materials, methods, applications and challenges*, Composites Part B: Engineering, Vol. 143, 2017, pp. 172–196, doi: 10.1016/j.compositesb.2018.02.012.

[3] **Bajaj P., Hariharan A., Kini A., Kürnsteiner P., Raabe D., Jägle E. A.,** *Steels in Additive Manufacturing: A review of their microstructure and properties*, Materials Science and Engineering A, Vol. 772, 138633, 2020, doi: 10.1016/j.msea.2019.138633.

[4] **Froes F. H., Dutta B.,** *The Additive Manufacturing (AM) of titanium alloys*, in Advanced Materials Research, Trans Tech Publications Ltd, 2014, pp. 19–25. doi: 10.4028/www.scientific.net/AMR.1019.19.

[5] **White J. P., Read N., Ward R. M., Mellor R., Attallah M. M.,** *Prediction of melt pool profiles for selective laser melting of AlSi10Mg alloy*, Materials Science and Technology Conference and Exhibition, MS and T, Vol 3, 2014, pp. 1985–1992.

[6] **Dutta B., Froes F. H. (Sam),** *The Additive Manufacturing (AM) of titanium alloys*, Metal Powder Report, Vol. 72(2), 2017, pp. 96–106, doi: 10.1016/j.mprp.2016.12.062.

[7] **Guo C., Li G., Li, S. Hu X., Lu H., Li X., Xu Z., Chen Y., Li Q., Lu J., Zhu Q.,** *Additive manufacturing of Ni-based superalloys: Residual stress, mechanisms of crack formation and strategies for crack inhibition*, Nano Materials Science, Vol. 5(1), 2023, pp. 53–77, doi: 10.1016/j.nanoms.2022.08.001.

[8] **Chittewar S. L., Patil N. G.,** *Surface integrity of conventional and additively manufactured nickel superalloys: A review*, Materials Today: Proceedings, 2021, pp. 701–708. doi: 10.1016/j.matpr.2020.10.614.

[9] **Hosseini E., Popovich V. A.,** *A review of mechanical properties of additively manufactured Inconel 718*, Additive Manufacturing, Vol. 30, 100877, 2019, doi: 10.1016/j.addma.2019.100877.

[10] **Wang J., Zhu R., Liu Y., Zhang L.,** *Understanding melt pool characteristics in laser powder bed fusion: An overview of single- and multi-track melt pools for process optimization*, Advanced Powder Materials, Vol. 2(4), KeAi Communications Co., 2023, doi: 10.1016/j.apmate.2023.100137.

[11] **Deshpande A.,** *Additive Manufacturing of Nickel Alloys,* Springer Handbook of Additive Manufacturing, Editors: E. Pei, A. Bernard, D. Gu, C. Klahn, M. Monzón, M. Petersen, and T. Sun, Springer International Publishing, 2023, pp. 655–669. doi: 10.1007/978-3-031-20752-5_39.

[12] **Nandhakumar R., Venkatesan K.,** *A process parameters review on selective laser melting-based additive manufacturing of single and multi-material: Microstructure, physical properties, tribological, and surface roughness*, Materials Today Communications, Vol. 35, 105538, 2023, doi: 10.1016/j.mtcomm.2023.105538.

[13] **Andreotta R., Ladani L., Brindley W.,** *Finite element simulation of laser additive melting and solidification of Inconel 718 with experimentally tested thermal properties*, Finite Elements in Analysis and Design, vol. 135, 2017, pp. 36–43, doi: 10.1016/j.finel.2017.07.002.

[14] **Khorasani M., Hossein Ghasemi A., Leary L., Cordova L., Sharabian L., Farabi E., Gibson I., Brandt M., Rolfe B.,** *A comprehensive study on meltpool depth in laser-based powder bed fusion of Inconel 718*, International Journal of Advanced Manufacturing Technology, Vol. 120(3–4), 2022, pp. 2345–2362, doi: 10.1007/s00170-021-08618-7.

[15] **Kumar A., Shukla M.,** *Numerical Modeling of Selective Laser Melting: Influence of Process Parameters on the Melt Pool Geometry*, Journal of Materials Engineering and Performance, Vol. 32(17), 2023, pp. 7998–8013, doi: 10.1007/s11665-022-07693-5.